Materials Advances

ROYAL SOCIETY OF CHEMISTRY

COMMUNICATION

View Article Online
View Journal | View Issue

Cite this: *Mater. Adv.*, 2023, 4, 1623

Received 12th December 2022, Accepted 2nd March 2023

DOI: 10.1039/d2ma01077a

rsc.li/materials-advances

High-performance anodes for aqueous Zn–iodine batteries from spent Zn–air batteries†

Xiaofeng Shan,[a] Yanqing Fu,*[ab] Dongdong Zhang,[a] Pan Li,[a] Weiyou Yang [a] and Qiliang Wei *[a]

Recycling spent batteries is of strategic importance from an environmental and economic standpoint. Herein, the discharge product of Zn–air batteries is re-used as a superior anode to facilitate the Zn stripping/plating process, inhibit dendrite growth, and alleviate the iodide crossover issue, thus endowing Zn–iodine batteries with enhanced electrochemical performance.

The substantial risks and increasing concerns from energy and environmental viewpoints in the past several decades have motivated people to develop and improve a variety of sustainable electrochemical energy technologies, such as rechargeable batteries, fuel cells, and supercapacitors.[1–5] Currently, Li-ion batteries (LIBs) are dominating the commercial rechargeable battery market, ranging from portable electronics and electric vehicles (EVs) to grid energy storage (GES) applications that benefit from their high energy density.[6–8] However, with the ever-increasing demand for energy and the environmental pollution burden, numerous concerns have arisen about the limited resources, high cost, insufficiency of power density, safety issues, and environmental impact of LIBs. Therefore, new concepts for electrochemical energy storage (EES) beyond LIBs are under intensive investigation.[9–11] Aqueous Zn–iodine batteries have emerged as a candidate for GES owing to their elemental abundance, safety, and low cost.[12–18] However, the high desolvation energy associated with the Zn stripping/plating process, the detrimental dendrite growth on the Zn anode, and the crossover of (poly)iodide species from the cathode to the Zn anode hinder their applications. The exploration of high-performance anodes is urgently required. Several strategies have been adopted to address these issues. For example, metal–organic framework (MOF)-based multifunctional membranes have been employed to restrict the crossover of iodide ion species in Zn//I_2 batteries;[19] we have recently demonstrated that the electrochemical performance of the Zn//I_2 battery can be enhanced using a Zn anode protected by a chemically-stable, fluorine-free cation exchange membrane, *i.e.*, sulfophenylated poly(phenylene)biphenyl (sPPB).[18] The protection mechanism of sPPB to repel the crossover of triiodide anions (I^{3-}) for the Zn–I_2 battery is based on the Donnan effect, with a negatively-charged backbone in sPPB. In addition, the construction of metal-fluorides, -oxides, -sulfides, and -phosphides on metal Zn surface has been reported as an alternative way to improve the electrochemical performance of Zn anodes by protecting the Zn from detrimental dendrite growth and side reactions in zinc-ion batteries (ZIBs).[20–25] Nonetheless, expensive or toxic materials and harsh experimental conditions are usually involved in fabricating these protection layers.

From a sustainability perspective, the recycling of spent batteries into a useful component of energy systems is of strategic importance for both environmental protection and economic aspects.[26–28] The alkaline Zn–air battery (ZAB) is a promising energy storage technology that has the advantages of low cost, eco-friendliness, and high energy density.[29–31] During discharge, a thin zinc oxide film is formed on the anode electrode. It will be very interesting to discover the potential applications of the Zn anode cycled from a discharged Zn–air battery (denoted as Zn-ZAB). Herein, we show that the Zn-ZAB electrode can directly serve as an efficient anode for neutral aqueous Zn//I_2 batteries. Furthermore, the Zn-ZAB is proved to simultaneously increase the Zn deposition kinetics, suppress Zn dendrites, and enhance the uniform plating/stripping of the Zn anode upon cycling, thus improving the electrochemical performance of Zn–I_2 batteries.

Fig. 1a shows a schematic illustration of the as-assembled aqueous Zn–air battery. On the cathode side, the Fe–N–C catalyst is used to facilitate the oxygen reduction reaction.[32] During the discharge process, the LED screen can be lit up, as shown in the inset of Fig. 1b, and the Zn anode is slowly oxidized to ZnO as in the equations below to form the ZnO-coated Zn:

[a] *Institute of Micro/Nano Materials and Devices, Ningbo University of Technology, Ningbo, 315211, P. R. China. E-mail: yanqing.fu92@gmail.com, qiliang.wei@nbut.edu.cn*

[b] *Laboratory of Infrared Material and Devices & Key Laboratory of Photoelectric Materials and Devices of Zhejiang Province, Advanced Technology Research Institute, Ningbo University, Ningbo, 315211, China*

† Electronic supplementary information (ESI) available. See DOI: https://doi.org/10.1039/d2ma01077a

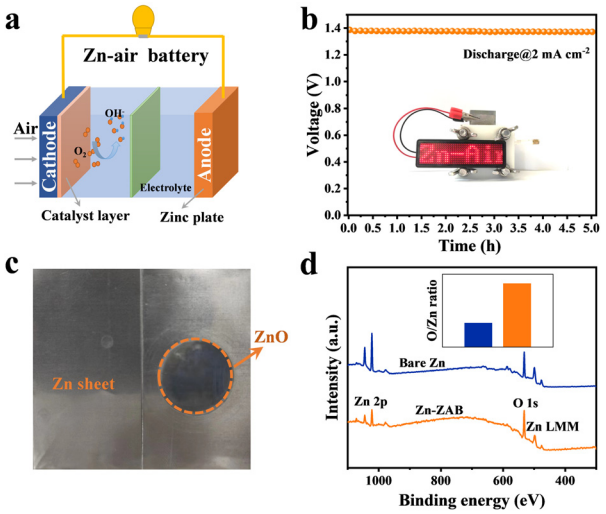

Fig. 1 (a) Schematic illustration of an as-assembled Zn–air battery. (b) Discharge profile of a Zn–air battery under 2 mA cm^{-2}. (c) Photograph of the bare Zn foil and the discharged Zn-ZAB electrode derived from (b). (d) XPS survey of the bare Zn and the Zn-ZAB electrodes (the inset shows the O/Zn ratio of the two electrodes).

$$Zn \rightarrow Zn^{2+} + 2e^{-} \quad (1)$$

$$Zn^{2+} + 4OH^{-} \rightarrow Zn(OH)_4^{2-} \quad (2)$$

$$Zn(OH)_4^{2-} \rightarrow ZnO + H_2O + 2OH^{-} \quad (3)$$

As an illustration, the Zn–air battery was discharged for 5 h at a current density of 2 mA cm^{-2} (Fig. 1b), which corresponds to an output capacity of 10 mA h cm^{-2}. After discharging, the Zn foil was dissembled and cleaned for the following experiments. From the photographs of the fresh Zn foil (left side of Fig. 1c) and the discharged Zn anode (right side of Fig. 1c), the dark hue of the zinc oxide film can be seen on the right side, different from its original metallic luster. XPS elemental analysis results of the bare Zn electrode and the Zn-ZAB are shown in Fig. 1d. It is obvious that both samples have Zn and O on the surface, and the relative oxygen content of the Zn-ZAB is more than double that of the bare Zn, showing that the Zn is covered by a thin film of zinc oxide.

The electrochemical behavior of bare Zn and the Zn-ZAB is first evaluated in symmetrical coin cells using 1 M $ZnSO_4$ as the electrolyte at a current density of 1.0 mA cm^{-2}. As shown in Fig. 2a, the bare Zn displays a fluctuating profile with a short lifetime of $<$80 h; by contrast, a stable plating/stripping process with a lower voltage hysteresis ($<$50 mV, Fig. S1, ESI†) and a prolonged cycling life span ($>$800 h) can be observed for the Zn-ZAB electrode. The rate performance of symmetric cells was also measured from 0.2 to 5.0 mA cm^{-2} (Fig. 2b). During the whole process, the Zn-ZAB electrode shows lower polarization in comparison with the bare Zn electrode. In particular, the voltage hysteresis of the Zn-ZAB electrode at a low current density of 0.2 mA cm^{-2} is $<$10 mV, significantly less than that of bare Zn (Fig. S2, ESI†), indicating a favorable Zn stripping/plating process for the Zn-ZAB electrode formed from waste

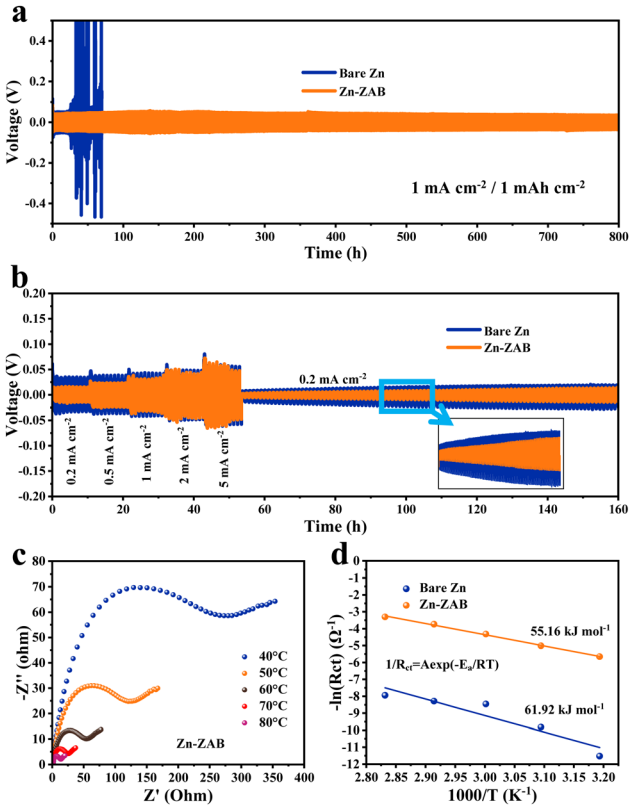

Fig. 2 (a) Cycling performance of symmetric cells with bare Zn and Zn-ZAB electrodes at a current density of 1.0 mA cm^{-2}. (b) Cycling performance of symmetric cells with bare Zn and Zn-ZAB electrodes at different current densities ranging from 0.2 to 5 mA cm^{-2}. (c) Nyquist plots at different temperatures of the Zn-ZAB electrode symmetric cells. (d) Corresponding Arrhenius curves and the calculated activation energies of bare Zn and Zn-ZAB electrodes.

ZABs. The charge transfer impedance of Zn^{2+} was investigated *via* electrochemical impedance spectroscopy (EIS) in symmetric cells under different temperatures from 40 to 80 °C (Fig. S3 and Fig. 2c, ESI†). The charge transfer resistance (R_{ct}) of the Zn-ZAB electrode is almost two orders of magnitude lower than that of bare Zn, indicating the favorable ion transfer at the interface between the electrolyte and the electrode in the Zn-ZAB electrode cells. In addition, the Zn-ZAB electrode cell has a high slope in the low-frequency region of the EIS curves, which suggests that Zn^{2+} is rapidly deposited during cycling at various temperatures.[23] The Arrhenius equation is used to calculate the activation energy (E_a), a measure of the energy barrier that electrochemical reactions must overcome, by fitting the R_{ct} under various temperatures. As shown in Fig. 2d, the activation energy of the Zn-ZAB electrode is calculated as 55.16 kJ mol^{-1}, lower than that of the bare Zn electrode (61.92 kJ mol^{-1}), indicating that the zinc oxide film improves the deposition kinetics and facilitates the transfer of Zn^{2+}. In addition, the wettability between the electrodes and the $ZnSO_4$ electrolyte was investigated and is displayed in Fig. S7 (ESI†), where the larger contact angle of 105.5° for bare Zn indicates its poor wettability, while a greatly reduced contact angle of 45.9° was

observed for Zn-ZAB, reflecting its remarkably improved wettability, which leads to a facilitated interaction between the electrolyte and the electrode.

Fig. S4 (ESI†) shows the cyclic voltammograms (CV) of typical Zn//I_2 coin-cells captured at 1.0 mV s^{-1}, respectively, with a bare Zn anode and a Zn-ZAB anode. Both curves feature the same redox peaks, with Zn-ZAB showing a slightly lower overpotential. The galvanostatic charge/discharge profiles of the bare Zn//I_2 cell and the Zn-ZAB//I_2 cell at 5C are displayed in Fig. 3a. It can be seen that the overpotential between the charge and discharge polarization curves of the Zn-ZAB//I_2 cell is lower than that of the bare Zn//I_2 cell, indicating that the solvation/desolvation energy barrier is facilitated by the thin zinc oxide film, which is consistent with the calculated activation energies using the Arrhenius equation (Fig. 2d). Generally, self-discharge is one issue that exists for the Zn//I_2 battery due to the shuttling of iodide species from the cathode to the anode; thus, further charge–discharge cycling was conducted at 1C, holding for 12 h after each full charge state. The ratio of the discharge capacity to the charge capacity (DC/CC capacity ratio) in the first 3 cycles is presented in Fig. 3b. It is clear that the Zn-ZAB//I_2 cell has a higher DC/CC ratio throughout the whole process than that of the bare Zn//I_2 cell, which indicates an efficient suppression of mobile of I_3^- species by the discharged ZAB-derived product (a thin oxide layer) on the Zn anode. The cycling performance operated at 5C is displayed in Fig. 3c, and the corresponding charge–discharge curves are shown in Fig. S5 and S6 (ESI†). Due to the protective layer of zinc oxide, the specific capacity of the Zn-ZAB//I_2 battery is maintained as 128 mA h g^{-1} after 350 cycles, which is clearly higher than that of the bare Zn-based Zn//I_2 battery (100 mA h g^{-1}). The rate performance of the Zn//I_2 batteries is shown in Fig. 3d. The specific capacity of the Zn-ZAB//I_2 battery achieved at 1C, 2C, 5C, 10C, 20C, and 30C is 205, 192, 167, 145, 120, and 92 mA h g^{-1}, respectively, and when the current density is reverted to 1C a high capacity of ~200 mA h g^{-1} is achieved, showing a good rate property. Comparing the rate performance between the bare Zn-based and Zn-ZAB-based Zn//I_2 batteries, it can be found that for low rates, the specific capacitance of Zn-ZAB//I_2 is much higher than that of bare-Zn//I_2. This indicates the facilitated kinetics of Zn^{2+} transfer for the formed zinc oxide in the Zn-ZAB electrode.[20] However, due to the insulating feature of zinc oxide, the electron conductivity of Zn-ZAB is limited; thus, when the current density reaches a high rate, the determining factor of the electrochemical performance most probably becomes to the electron conductivity instead of the Zn^{2+} transfer kinetics. To analyze the cycling stability of the full cell, the EIS of the Zn–I_2 battery and the morphology of the anodes before and after cycling were characterized, as shown in Fig. 3e. From the EIS curves in Fig. 3e, the R_{ct} of the bare Zn//I_2 battery and the Zn-ZAB//I_2 battery before cycling is 1 Ω and 2.5 Ω, respectively. After 350 cycles, the R_{ct} of the Zn-ZAB//I_2 battery is maintained at 1.5 Ω, while the R_{ct} of the bare Zn–I_2 battery rises to 5 Ω, highlighting the benefit of the protecting zinc oxide film on the surface.

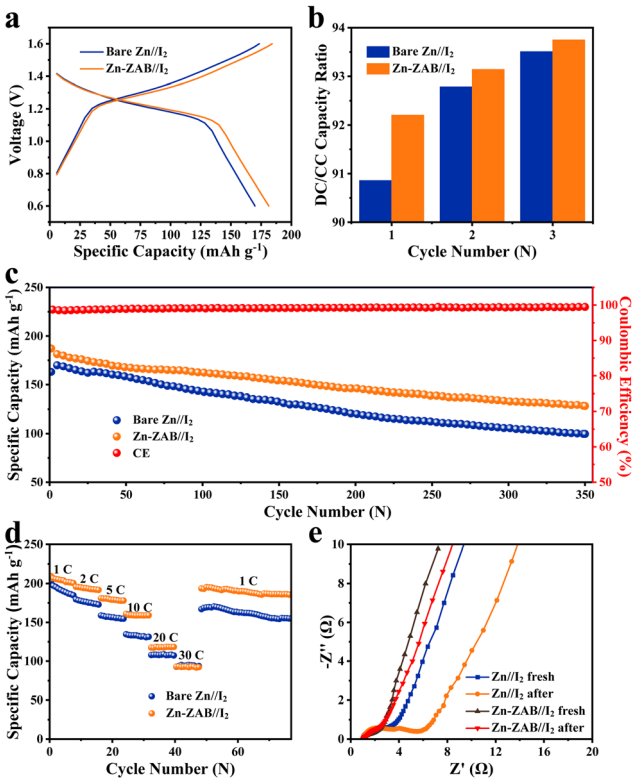

Fig. 3 (a) Galvanostatic discharge–charge profiles of the bare Zn//I_2 battery and the Zn-ZAB//I_2 battery obtained in the 5th cycle. (b) Coulombic efficiency of the Zn//I_2 and Zn-ZAB//I_2 batteries with 12 h holding after each full charge state. (c) Cycling performance of the Zn//I_2 and Zn-ZAB//I_2 batteries at 5C. (d) Rate performance of the bare Zn//I_2 battery and the Zn-ZAB//I_2 battery. (e) Nyquist plots of the Zn//I_2 battery and the Zn-ZAB//I_2 battery before and after cycling.

The protective mechanism of the zinc oxide film for the Zn anode is presented in Fig. 4a based on the electrochemical performance discussed above. Without the protective layer, Zn dendrites are generated during cycling, and negatively charged iodide species can easily shuttle to the anode side, accelerating the side reactions.[19] With the protective zinc oxide layer, the formation of Zn dendrites can be efficiently alleviated; at the same time, the negatively charged dense oxide layer (the zeta potential is measured as −0.554 mV, see Fig. S8, ESI†) can also serve as a blocking layer to mitigate the side reactions on the anode due to the physical resistance and the electrostatic repulsion effect. From SEM images of fresh electrodes (Fig. 4b and e) and post-mortem electrodes (Fig. 4c, d, f and g), the difference between bare Zn and Zn-ZAB can clearly be observed. Before cycling, the surface of the bare Zn is smooth, and the Zn-ZAB formed from the ZABs shows significant surface roughness. After 350 cycles, it appears that dendritic structures are forming on the bare Zn electrode, while the morphology of the Zn-ZAB becomes more uniform with dendrites not visible. This morphology evolution once again explains the reason for the superior performance of the Zn-ZAB-based batteries. Therefore, all of these results confirm that our strategy for recycling of the Zn anodes from spent alkaline ZABs to make high-performance anodes for neutral Zn–I_2 batteries is feasible.

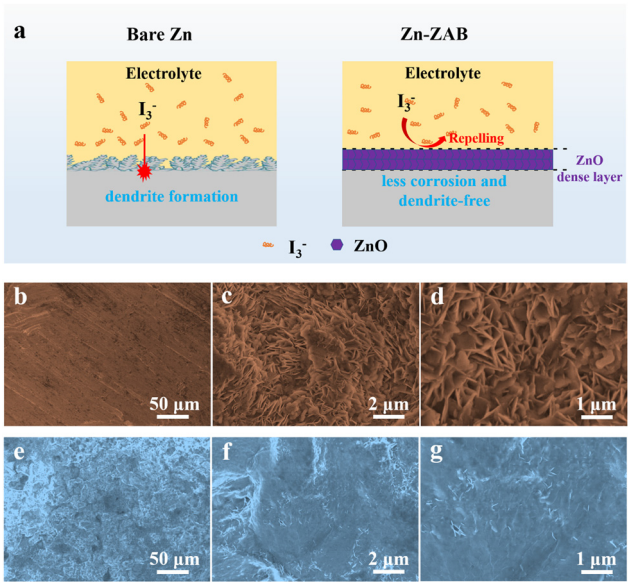

Fig. 4 (a) Schematic diagram of the protective mechanism of the zinc oxide film for bare Zn and Zn-ZAB electrodes for the Zn–I_2 battery. (b–d) SEM images of the bare Zn electrode before (b) and after cycling (c and d). (e–g) SEM images of the Zn-ZAB electrode before (e) and after cycling (f and g).

In summary, we successfully re-use Zn anodes from spent Zn–air batteries as anodes in neutral Zn//I_2 battery systems. The thin layer of zinc oxide over Zn not only facilitates the transfer of Zn^{2+} and improves the deposition kinetics but also increases the specific capacitance and the lifespan of the Zn//I_2 battery by suppressing the growth of Zn dendrites and the shuttling of iodide species. These results indicate that recycling the anodes of Zn–air batteries can be an effective approach to making high-performance anodes for neutral Zn-based aqueous battery systems.

X. Shan: methodology, visualization, writing – review and editing. Y. Fu: conceptualization, methodology, visualization, writing – review and editing. D. Zhang: methodology, visualization, writing – review and editing. P. Li: methodology, visualization. W. Yang: funding acquisition, conceptualization, writing – review and editing, supervision. Q. Wei: funding acquisition, conceptualization, methodology, visualization, writing – review and editing, supervision.

This work was supported by the National Natural Science Foundation of China (NSFC, Grant No. 51972178), the Natural Science Foundation of Ningbo (2022J139), the Ningbo Yongjiang Talent Introduction Programme (2022A-227-G), and start-up funding of the Ningbo University of Technology (2022KQ05). The authors would like to thank Rongqi Xia from Shiyanjia Lab (www.shiyanjia.com) for the zeta-potential measurement.

Conflicts of interest

The authors declare no competing interests.

Notes and references

1 M. J. Lee, J. Han, K. Lee, Y. J. Lee, B. G. Kim, K.-N. Jung, B. J. Kim and S. W. Lee, *Nature*, 2022, **601**, 217–222.
2 M. Winter and R. J. Brodd, *Chem. Rev.*, 2004, **104**, 4245–4270.
3 J. Fan, M. Chen, Z. Zhao, Z. Zhang, S. Ye, S. Xu, H. Wang and H. Li, *Nat. Energy*, 2021, **6**, 475–486.
4 M. Salanne, B. Rotenberg, K. Naoi, K. Kaneko, P.-L. Taberna, C. P. Grey, B. Dunn and P. Simon, *Nat. Energy*, 2016, **1**, 1–10.
5 Q. Wei, Y. Fu, G. Zhang, D. Yang, G. Meng and S. Sun, *Nano Energy*, 2019, **55**, 234–259.
6 B. Wu, X. Yang, X. Jiang, Y. Zhang, H. Shu, P. Gao, L. Liu and X. Wang, *Adv. Funct. Mater.*, 2018, **28**, 1803392.
7 R. Zhan, X. Wang, Z. Chen, Z. W. Seh, L. Wang and Y. Sun, *Adv. Energy Mater.*, 2021, **11**, 2101565.
8 Y. Fu, Q. Wei, G. Zhang and S. Sun, *Adv. Energy Mater.*, 2018, **8**, 1703058.
9 D. Chao, W. Zhou, F. Xie, C. Ye, H. Li, M. Jaroniec and S.-Z. Qiao, *Sci. Adv.*, 2020, **6**, eaba4098.
10 A. Luntz, *J. Phys. Chem. Lett.*, 2015, **6**, 300–301.
11 J. Ni, A. Dai, Y. Yuan, L. Li and J. Lu, *Matter*, 2020, **2**, 1366–1376.
12 F. Wang, O. Borodin, T. Gao, X. Fan, W. Sun, F. Han, A. Faraone, J. A. Dura, K. Xu and C. Wang, *Nat. Mater.*, 2018, **17**, 543–549.
13 H. Pan, B. Li, D. Mei, Z. Nie, Y. Shao, G. Li, X. S. Li, K. S. Han, K. T. Mueller and V. Sprenkle, *ACS Energy Lett.*, 2017, **2**, 2674–2680.
14 W. Wu, C. Li, Z. Wang, H.-Y. Shi, Y. Song, X.-X. Liu and X. Sun, *Chem. Eng. J.*, 2022, **428**, 131283.
15 L. Ma, Y. Ying, S. Chen, Z. Huang, X. Li, H. Huang and C. Zhi, *Angew. Chem.*, 2021, **133**, 3835–3842.
16 D. Lin and Y. Li, *Adv. Mater.*, 2022, 2108856.
17 Y. Yang, S. Liang and J. Zhou, *Curr. Opin. Electrochem.*, 2021, **30**, 100761.
18 Q. Wei, E. Schibli, B. Chen and S. Holdcroft, *Energy Adv.*, 2022, **1**, 606–612.
19 H. Yang, Y. Qiao, Z. Chang, H. Deng, P. He and H. Zhou, *Adv. Mater.*, 2020, **32**, 2004240.
20 X. Xie, S. Liang, J. Gao, S. Guo, J. Guo, C. Wang, G. Xu, X. Wu, G. Chen and J. Zhou, *Energy Environ. Sci.*, 2020, **13**, 503–510.
21 X. He, Y. Cui, Y. Qian, Y. Wu, H. Ling, H. Zhang, X.-Y. Kong, Y. Zhao, M. Xue and L. Jiang, *J. Am. Chem. Soc.*, 2022, **144**, 11168–11177.
22 Y. An, Y. Tian, C. Liu, S. Xiong, J. Feng and Y. Qian, *ACS Nano*, 2021, **15**, 15259–15273.
23 P. Cao, X. Zhou, A. Wei, Q. Meng, H. Ye, W. Liu, J. Tang and J. Yang, *Adv. Funct. Mater.*, 2021, **31**, 2100398.
24 J. Y. Kim, G. Liu, G. Y. Shim, H. Kim and J. K. Lee, *Adv. Funct. Mater.*, 2020, **30**, 2004210.
25 Y. Yang, C. Liu, Z. Lv, H. Yang, Y. Zhang, M. Ye, L. Chen, J. Zhao and C. C. Li, *Adv. Mater.*, 2021, **33**, 2007388.
26 X. Zhang, L. Li, E. Fan, Q. Xue, Y. Bian, F. Wu and R. Chen, *Chem. Soc. Rev.*, 2018, **47**, 7239–7302.

27 M. Fan, X. Chang, Q. Meng, L. J. Wan and Y. G. Guo, *SusMat*, 2021, **1**, 241–254.
28 Q. Wei, X. Yang, G. Zhang, D. Wang, L. Zuin, D. Banham, L. Yang, S. Ye, Y. Wang and M. Mohamedi, *Appl. Catal., B*, 2018, **237**, 85–93.
29 X. Zhu, C. Hu, R. Amal, L. Dai and X. Lu, *Energy Environ. Sci.*, 2020, **13**, 4536–4563.
30 Z. Zhao, X. Fan, J. Ding, W. Hu, C. Zhong and J. Lu, *ACS Energy Lett.*, 2019, **4**, 2259–2270.
31 Q. Wei, G. Zhang, X. Yang, Y. Fu, G. Yang, N. Chen, W. Chen and S. Sun, *J. Mater. Chem. A*, 2018, **6**, 4605–4610.
32 H. Zhang, S. Hwang, M. Wang, Z. Feng, S. Karakalos, L. Luo, Z. Qiao, X. Xie, C. Wang and D. Su, *J. Am. Chem. Soc.*, 2017, **139**, 14143–14149.